Motion Planning for the Virtual Bronchoscopy

Jan Rosell, Alexander Pérez, Paolo Cabras and Antoni Rosell

Abstract— **Bronchoscopy is an interventional medical procedure employed to analyze the interior side of the human airways, clear possible obstructions and biopsy. Using a 3D reconstruction of the tracheobronchial tree, Virtual Bronchoscopy (VB) may help physicians in the exploration of peripheral lung lesions. We are developing a haptic-based navigation system for the VB that allows the navigation within the airways using a haptic device whose permitted motions mimics those done with the real bronchoscope. This paper describes the motion planning module of the system devoted to plan a path from the trachea to small peripheral pulmonary lesions, that takes into account the geometry and the kinematic constraints of the bronchoscope. The motion planner output is used to visually and haptically guide the navigation during the virtual exploration using the haptic device. Moreover, physicians can get useful information of whether the peripheral lesions can effectively be reached with a given bronchoscope or of which is the nearest point to the lesion that can be reached.**

I. Introduction

Lung cancer diagnosis usually requires bronchoscopy for the biopsy of lesions identified by chest X-ray or a thorax computed tomography (CT), although for small peripheral pulmonary lesions, percutaneous needle aspiration cytology or biopsy are used. These techniques have a high success rates but a risk of pneumothorax, among other problems. For this reason, transbronchial biopsy using ultrathin bronchoscopes is becoming a good alternative since they can be inserted under direct vision into more peripheral bronchi than conventional bronchoscopes. The identification of the accessible bronchial routes to reach the small peripheral pulmonary lesions is, however, not easy during limited examination time, and therefore the availability of a Virtual Bronchoscopy (VB) system may be of great help [1].

VB is a computer-generated 3D reconstruction technique that allows physicians to explore the tracheobronchial tree to help locating the diseased zone (e.g. by making the virtual bronchial tube semi-transparent so as to make the lymph node visible), evaluate whether it is necessary to proceed with the real bronchoscopy and automatically plan a path within the 3D model [2]. One of the weak points of the current VB systems is that they only provide an exploration made by a camera flight passing through pre-computed points, or controlled with the keyboard or mouse, i.e. the geometry and kinematic constraints of the bronchoscope are neglected. Therefore, on the one hand no correspondence exists with the real movements the physician would do with a real bronchoscope, and on the other no information is provided of whether a peripheral lesions can effectively be reached with a given bronchoscope, or of which is the nearest point to that lesion that can be reached. In order to be able to answer these questions, and to make lung exploration as realistic as possible, as if physicians were really handling a bronchoscope, we are developing a haptic-based navigation system for the VB that allows the exploration of the airways using a haptic device whose permitted motions mimic those done with the real bronchoscope [3]. Moreover, the system is designed to provide a visual and haptic guidance to selected peripheral lesions, based on the results of a motion planning module that is proposed in the present paper.

After this introduction, the paper is structured as follows. Section II presents some related work and Section III presents the framework, the problem statement and the solution overview. Then Section IV deals with modelling issues and Section V introduces the planning proposal. Finally, Section VI shows some results and Section VII presents the conclusions.

II. Related work

Motion planning for the Virtual Bronchoscopy has been, up to now, only thought for fly-through animations, i.e. to find a path for a point-camera from the trachea to a goal region neglecting the geometry and kinematic constraints of the bronchoscope. Kiraly et al. [4] built a skeleton from the segmented CT-images and improved it by eliminating false branches and performing a branch-centering process, then proceed with a sub-voxel interpolation using splines, and finally derived the viewing directions. A similar, though simpler, approach was presented in [5].

A bronchoscope (or videobronchoscope) is a long, thin, flexible tube attached to a CCD camera. Some authors in the path planning area have coped with the problem of planning paths for deformable linear objects, like the work of Moll and Kavraki [6], suggested for the planning of surgical suturing, or the work of Gayle et al. [7], applied in performing path planning of catheters in liver chemoembolization by treating the problem as a constrained dynamic simulation problem. This last approach could be applied to the virtual bronchoscopy to consider the geometry of the bronchoscope, although the kinematic constraints that condition the bronchoscope steering should be included somehow.

The motion of the camera attached at the tip of the bronchoscope has three degrees of freedom (the rotation

This work was partially supported by the Spanish Government through the projects PI09/90088, PI09/90917, DPI2008-02448 and DPI2010-15446.

J. Rosell, A. Pérez and P. Cabras are with the Institute of Industrial and Control Engineering (IOC) - Technical University of Catalonia (UPC), Barcelona, Spain jan.rosell@upc.edu. A. Pérez is also with the Escuela Colombiana de Ingeniería "Julio Garavito", Bogotá D.C.. A. Rosell is with the Servei de Pneumologia, Direcció Clínica de Malalties Respiratòries, Grup de Recerca Pneumològica-IDIBELL, Hospital Universitari de Bellvitge, Barcelona, Spain.

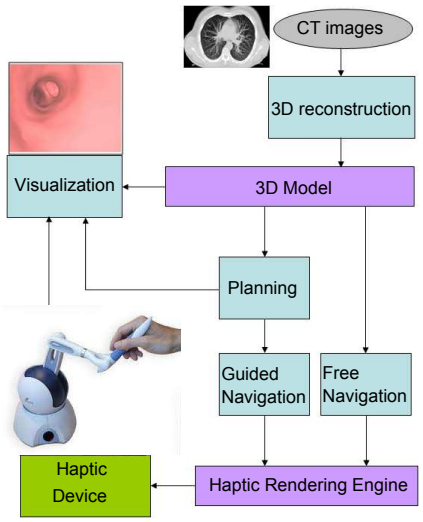

Fig. 1. Modules involved in the haptic guided VB system.

around the tube axis, the advance along it and the bending of the tip) and it is affected by non-holonomic constraints. Similar motion constraints are found in the planning of motions for highly flexible, bevel-tip needles that move along curved trajectories within tissue when a forward pushing force is applied. For this problem, Lobaton et al. [8] constructed a Probabilistic Roadmap (PRM) by sampling circles of constant curvature and then generating feasible transitions between the sampled circles with a closed-form formula for 2D and 3D workspaces, and Patil and Alterovitz [9] proposed a Rapidly-exploring Random Tree (RRT) with a reachability-guided sampling heuristic [10] customized for that problem. This last proposal could be adapted for the bronchoscopy (to take into account that for the bronchoscopy the workspace is the tracheobronchial tree which is a highly constrained space without obstacles), using some planning RRT-based approaches like [11] or [12].

Nevertheless, to be used as a guiding aid, the solutions provided by feedback motion planners, like those based on potential functions, seem better than graph-based approaches since they can provide information of the direction to follow to reach the goal from wherever the user may be. To take into account non-holonomic constraints, these approaches either locally deform the potential fields with respect to the non-holonomic constraints of the system [13], or define a feedback control law to continually align the velocity vector of the robot with the direction of the navigation function gradient [14]. The present proposal is a feedback motion planner for the virtual bronchoscopy that takes into account the geometry and kinematic constraints of the bronchoscope.

III. Framework, problem statement and overview

The haptic-based navigation system for the VB that we are developing is schematically illustrated in Fig. 1. Starting with a stack of CT images of the chest, the 3D reconstruction module generates a triangular mesh that represents the 3D model of the tracheobronchial tree that is shown by the visualization module both from the inside and from the outside. The free-navigation module, introduced in [3], allows a realistic navigation within the airways by using a haptic device whose motions have been constrained to mimic those done with a real bronchoscope. Moreover, these motions can be modulated, facilitating some directions and hampering others, if the guided navigation module is used instead. The input of the guided navigation module comes from the planning module, which is the main focus of this paper, and whose requirements are as follows.

Given a model of the tracheobronchial tree and of the bronchoscope (including its kinematic constraints), and the specification of a peripheral pulmonary lesion, the planning module has to provide, for any location where the user might be, the motion to be followed to reach the lesion, and information of whether it can effectively be reached with a given bronchoscope or otherwise which is the nearest point to the lesion that can be reached.

The proposed method, detailed in Section V, is based on: 1) the computation of a navigation function over a 3D grid defined in the interior of the tracheobronchial tree such that results in high clearance geometric paths; and 2) the definition of a procedure (based on the previous step and that takes into account the geometry of the bronchoscope and its non-holonomic kinematic constraints) to iteratively advance the bronchoscope towards the goal along a collision-free path, maximizing the clearance and minimizing the changes in the values commanded.

IV. Task modelling

A. Tracheobronchial tree

To obtain a 3D image representing the tracheobronchial tree, a gray-scale morphological reconstruction method, based on the works of Kiraly et al. [15] and Babin et al. [16], is applied to the stack of 2D images that CT scanners provide. For visualization purposes, a three-dimensional triangular mesh that wraps the voxels with gray level below a given threshold is generated using the AMIRA software [17] and represented as a VRML file. For planning purposes the 3D image is binarized and a clearance map is computed by labeling the voxels pertaining to the interior of the bronchi with the L1 distance to the walls. Then, all these labeled voxels are represented as a graph (considering Manhattan neighborhood) using the Boost Graph library.

B. Goal regions

The peripheral lesions are the regions where the path to be planned must end; they are identified by the physicians on the CT images and represented as spheres on the VRML file (see Fig. 7b). A procedure is run to find all the voxels of the bronchi inside the sphere and determine the voxel which is nearest to its center, called the goal voxel.

C. The bronchoscope

Fig. 2 shows a bronchoscope. The motions of its flexible tip (approximately its last 2.5 cm) are controlled by the handle and allow the routing through the bronchi as it is introduced. These motions can be well described if the tip

Fig. 2. Degrees of freedom of a bronchoscope: Advance Δz, twist α and bending β.

TABLE I
DH-PARAMETERS

	α_{DH}	a	θ	d
link 0	0.0	0.0	$\theta_0 = \alpha$	0.0
links 1 to n	0.0	l	$\theta_i = \xi$	0.0

is modelled as a kinematic chain (Fig. 3a) composed of a set of $n+1$ equal links with coupled joints, except for the first link that is different and its joint is not coupled. The DH-parameters are shown in Table I, where the joint angles θ_0 and θ_i $\forall i = 1 \ldots n$ are named as α and ξ, and the total bending due to the coupled joints is named β, i.e. $\beta = n\xi$. The angles α and β are called the twist and the bending of the bronchoscope. A fixed transform is added to define the base of the chain with the Z_b-axis pointing in the opposite direction of the chain. The camera is located at the tip of the bronchoscope, looking towards the $-Z_t$-direction.

Geometrically, the first link (link 0) is a sphere of radius l; the other links (from link 1 to n) are modelled with two spheres (called base and end) of radius l connected with a cylinder of both radius and height also equal to l (Fig. 3b). The TCP (Tool Center Point) is set to the center of the end sphere of the last link of the robot. The current model has 11 joints (i.e. $n = 10$) and $l = 1$mm and the values of α and β vary (in degrees) within the ranges $\texttt{Range}(\alpha) = [-60, 90]$ and $\texttt{Range}(\beta) = [-90, 120]$, as shown in Fig. 3c (these parameters are easily customizable using an input file in XML format).

The motions of the bronchoscope can then be described with the following (coupled) three degrees of freedom (Figs. 2 and 3a):

1) *The twist motion about the tube axis:* It is produced by the rotation of the bronchoscope handle. It is modelled as a change in the angle α, i.e. in the first joint value.
2) *The bending of the tip:* It is obtained by turning a wheel. It is modelled as a change in the value ξ of the coupled joints, being the total bending equal to $\beta = n\xi$.
3) *The forward/backward motion of the tube along its axis:* It is performed by pushing and pulling the bronchoscope handle. It is modelled by an increment Δz applied to the base of the bronchoscope that produces a negative rotation of an angle $\Delta\beta$ about the X_C-axis (Fig. 3a):

$$\Delta\beta = \frac{\Delta z}{d} = \frac{2\Delta z \sin(\xi/2)}{l\cos(\xi/2)}$$

For the particular case of $\xi = 0$ (i.e. the tip is totally extended), it corresponds to a rectilinear translational motion along the Z_b-axis.

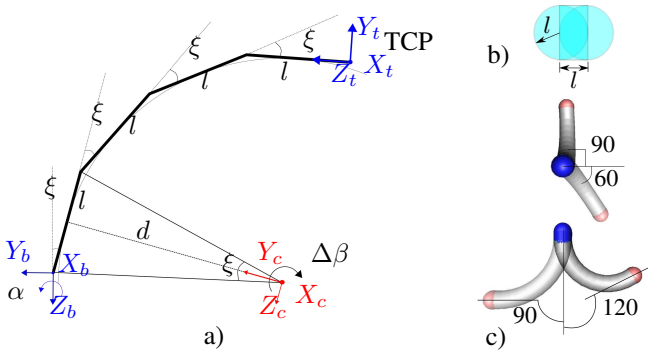

Fig. 3. a) Wireframe model of the bronchoscope for $n = 4$; b) A bronchoscope link c) Limits of the twist and bending angles.

Algorithm 1 Bronchoscope kinematics

Require:
$(\Delta z, \alpha, \beta)$: Advance step, twist angle and bending angle
T_{base_i}: Configuration of the bronchoscope base
n: number of coupled joints
l: link length
$T_{kin}(\theta_0, \theta_1, ..., \theta_n)$: Direct kinematics of the chain
Ensure:
$T_{TCP_{i+1}}$: New configuration of the bronchoscope TCP

1. $\xi = \beta/n$
2. $d = \frac{l\cos(\xi/2)}{2\sin(\xi/2)}$
3. $\Delta\beta = \frac{\Delta z}{d}$
4. $T_\alpha = \begin{bmatrix} \cos\alpha & -\sin\alpha & 0 & 0 \\ \sin\alpha & \cos\alpha & 0 & 0 \\ 0 & 0 & 1 & 0 \\ 0 & 0 & 0 & 1 \end{bmatrix}$
5. $T_C = \begin{bmatrix} 1 & 0 & 0 & 0 \\ 0 & \cos\xi & -\sin\xi & d \\ 0 & \sin\xi & \cos\xi & -l/2 \\ 0 & 0 & 0 & 1 \end{bmatrix}$
6. $T_{\Delta\beta} = \begin{bmatrix} 1 & 0 & 0 & 0 \\ 0 & \cos\Delta\beta & -\sin\Delta\beta & 0 \\ 0 & \sin\Delta\beta & \cos\Delta\beta & 0 \\ 0 & 0 & 0 & 1 \end{bmatrix}$
7. $T_{base_{i+1}} = T_{base_i} T_\alpha T_C T_{\Delta\beta} T_C^{-1} T_\alpha^{-1}$
8. $T_{TCP_{i+1}} = T_{base_{i+1}} T_{kin}(\alpha, \xi, .., \xi)$

return $T_{TCP_{i+1}}$

Algorithm 1 shows how to compute the transformation of the TCP of the bronchoscope after an advance motion of a Δz step, given the twist and bending angles.

D. Collision checking and distance computation

In order to determine if a link L_i is in collision the following steps are performed:

1) Find the voxel $v(L_i)$ that contains the center of the base sphere of the link (for the last link this is repeated for the end sphere, too).

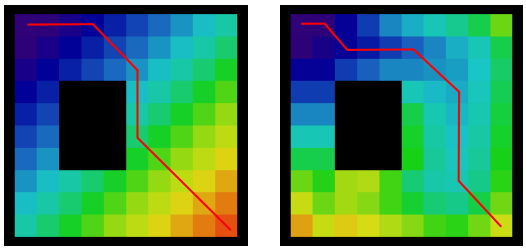

Fig. 4. Paths on a 2D space from an initial cell at the bottom-right corner to the goal cell at the top-left one, computed with the NF1 function (left) and the clearance-based NF1 function (right).

2) Verify if its clearance value $cl(v(L_i))$, computed as the L1 distance to the walls, satisfies:

$$cl(v(L_i)) \leq \frac{l}{s} \tag{1}$$

being s the size of the largest voxel side.

If condition (1) is satisfied the link is in collision and the bronchoscope is in a non-free configuration. When no link is in collision, the bronchoscope is in a free configuration and a distance value is associated to it. This distance value is computed as the sum of all the clearances computed for the collision-checking process.

V. Motion Planning

A. Clearance-based Navigation Function

Navigation functions are local minima-free potential function computed over a grid. The navigation function NF1 [18] is obtained by computing the L1 distances from a cell of the grid (the goal) by a wavefront propagation (Fig. 4 left).

The problem of the paths obtained with the NF1 navigation function is that they may graze the obstacles. In order to alleviate this problem, we have implemented a variant of the NF1 navigation function where the potential being propagated is decreased by a value proportional to the clearance. Let d_j be the potential of a given node j, d_i that of the neighbor node i being expanded, c_j be the clearance of node j (i.e. the L1 distance to the obstacles), and C_{max} a clearance threshold. Then, staring with a zero potential at the goal cell:

$$d_j = \begin{cases} d_i + 1 - \frac{c_j}{C_{max}} & \text{if } c_j < 0.9\, C_{max} \\ d_i + 0.1 & \text{otherwise} \end{cases} \tag{2}$$

Any visited node j may be revisited from other expanding neighbor nodes. The potential d_j is updated whenever the new expanding neighbor node results in a lower d_j value.

The clearance-based NF1 navigation function is a local-minima free potential that results in paths with a high clearance (Fig 4 right). It is computed on the tracheobronchial tree starting at the goal voxel (as computed in Section IV-B) and using C_{max} as half the maximum distance to the walls (it has been efficiently implemented using the Boost Graph functions). The potential values computed by the clearance-based NF1 navigation function will be called NF1 values.

B. Best-motion selection

To evaluate a control (α and β values) applied to advance the bronchoscope a Δz from a given configuration, a cost function is defined that verifies whether the resulting new configuration is: a) closer to the goal; b) has a better clearance and c) does not require a big change in the alpha value. The selection of the best possible motion is approximated by choosing it among a set S of 121 pairs of values (α, β). These values are obtained by sweeping the whole range of α and a subset of the range of β centered at the value β_0 corresponding to the current configuration:

$$\mathbf{c}_{(i,j)} = (\alpha_i, \beta_j) = (i\delta\alpha, \beta_0 + j\delta\beta) \;\; i,j \in \mathbb{Z}\ ,\ i,j \in [-5,5] \tag{3}$$

with $\delta\alpha = \texttt{Range}(\alpha)/10$ and $\delta\beta = 5°$ (if $\beta \notin \texttt{Range}(\beta)$ then $\mathbf{c}_{(i,j)}$ is not considered).

Let $S_{free} \subseteq S$ be the subset of pairs of values (α, β) that result, after advancing a step Δz, in a collision-free configuration, and let $S_{valid} \subseteq S_{free}$ be the subset that also satisfy that the TCP of the bronchoscope ends at a voxel with a lower NF1 value. For all pairs of values $(\alpha, \beta) \in S_{valid}$ the following costs are computed:

K_{NF1}: Cost that evaluates the decrease in the NF1 function. Let $\text{TCP}_{\text{NF1}}(\mathbf{c}_{(i,j)})$ be the value of the NF1 function at the voxel occupied by the TCP of the bronchoscope after a Δz is applied with the pair $\mathbf{c}_{(i,j)} \in S_{valid}$, and let $m_{NF1} = \min_{\forall \mathbf{c}_{(i,j)} \in S_{valid}} \text{TCP}_{\text{NF1}}(\mathbf{c}_{(i,j)})$ and $M_{NF1} = \max_{\forall \mathbf{c}_{(i,j)} \in S_{valid}} \text{TCP}_{\text{NF1}}(\mathbf{c}_{(i,j)})$, then the cost K_{NF1} is defined as:

$$K_{\text{NF1}}(i,j) = \frac{\text{TCP}_{\text{NF1}}(\mathbf{c}_{(i,j)}) - m_{\text{NF1}}}{M_{\text{NF1}} - m_{\text{NF1}}} \tag{4}$$

The smaller K_{NF1}, the better, i.e. it moves the TCP of the bronchoscope closer to the goal (that has a zero NF1 value).

K_{cl}: Cost that evaluates whether the applied motion improves the clearance at the TCP of the bronchoscope. Let $\mathbf{p}(v_0)$ and $cl(v_0)$ be the coordinates of the voxel closest to the TCP of the bronchoscope and its clearance, respectively, and $\mathbf{p}(v_k)$ and $cl(v_k)$ those of one of the 26-neighbors of v_0. Then the gradient of the clearance is defined as:

$$\mathbf{g} = \sum_{k=1}^{26} (\mathbf{p}(v_k) - \mathbf{p}(v_0))(cl(v_k) - cl(v_0)) \tag{5}$$

Let $\mathbf{p}^{(i,j)}(v_0)$ be the position of the voxel that contains the TCP of the bronchoscope after a Δz is applied with the pair (α_i, β_j), and let this position be called a *look-at point*. Let also $\mathbf{q}(i,j) = \frac{\mathbf{p}^{(i,j)}(v_0) - \mathbf{p}(v_0)}{\|\mathbf{p}^{(i,j)}(v_0) - \mathbf{p}(v_0)\|}$ be the resulting unitary direction of motion of the TCP. Then, to evaluate if the bronchoscope is moving towards a position with more clearance, the dot product of the motion direction with the distance gradient is computed:

$$\text{cg}(i,j) = \begin{cases} \mathbf{q}(i,j) \cdot \mathbf{g} & \text{if } \mathbf{q}(i,j) \cdot \mathbf{g} > 0 \\ 0 & \text{otherwise} \end{cases} \tag{6}$$

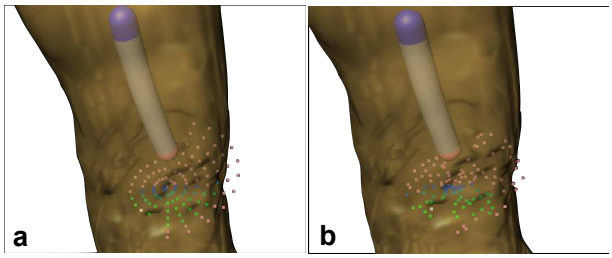

Fig. 5. Look-at points: Motions that produce an increase of the NF1 value of the TCP are discarded and the corresponding look-at points are painted in light red. Those that produce a decrease are candidates and are colored from blue to green as a function of increasing K. The motion with the best cost has the corresponding look-at point colored in white.

Finally, let $m_{cg} = \min_{\forall \mathbf{c}_{(i,j)} \in S_{valid}} \text{cg}(i,j)$ and $M_{cg} = \max_{\forall \mathbf{c}_{i,j} \in S_{valid}} \text{cg}(i,j)$. Then the cost K_{cl} is defined as:

$$K_{cl}(i,j) = 1 - \frac{\text{cg}(i,j) - m_{cg}}{M_{cg} - m_{cg}} \quad (7)$$

The smaller K_{cl}, the better, i.e. it moves towards configurations with more clearance.

K_α: Cost that weights both the changes in α (no big changes are desirable) and the absolute value of α (small values of α are preferred, for ergonomic reasons, when the bending is small; when the bending is not small the value of α is not a choice but is determined by the geometry of the bronchi).

$$K_\alpha(i,j) = 0.5(1 - |\hat{\beta}_j|)|\hat{\alpha}_i| + 0.5|(\hat{\alpha}_i - \hat{\alpha}_0)/2| \quad (8)$$

with $\hat{\alpha}, \hat{\beta} \in [-1, 1]$. The smaller K_α, the better, i.e. small changes in α and/or small absolute values of α.

The final cost is a weighted average of the three cost values:

$$K(i,j) = \omega_{\text{NF1}} K_{NF1}(i,j) + \omega_{cl} K_{cl}(i,j) + \omega_\alpha K_\alpha(i,j) \quad (9)$$

The value of K is in the range $[0, 1]$ because K_{NF1}, K_{cl} and K_α are in this range and the selected weights are positive and satisfy $\omega_{\text{NF1}} + \omega_{cl} + \omega_\alpha = 1$. The best motion is that which produces a lower value of K.

As an example, Fig. 5 shows the look-at points colored as a function of the cost K. In Fig. 5a the values selected in (3) are used, whereas in Fig. 5b random offsets within the ranges $\pm\frac{\delta\alpha}{2}$ and $\pm\frac{\delta\beta}{2}$ have been added to the values of α_i and β_j, respectively, except for $\mathbf{c}_{(0,0)}$, to better cover the range of candidate values.

Fig. 6 show, the distances (as computed in section IV-D) and the values of the twist α recorded during the execution of a path from the trachea to a peripheral lesion, using different values of the weights. It is shown that, besides the advance towards the goal induced by K_{NF1}, the consideration of K_{cl} and K_α allow a better quality paths, i.e. with more clearance and less twist changes.

C. The algorithm

Algorithm 2 computes a path for the bronchoscope from the initial configuration to a final configuration, i.e. with the TCP inside the goal voxel. The algorithm can be automatically executed, prior to the virtual exploration using the haptic device, to allow the visualization of the path and to give the information of whether the lesion can effectively be reached or of which is the nearest point to the lesion that can be reached. Step 3.4. of the algorithm is performed by Algorithm 1 using a smaller advance step $\delta z < \Delta z$ and the corresponding interpolated twist and bending angles $\alpha_0 + (\alpha_i - \alpha_0)\frac{\delta z}{\Delta z}$ and $\beta_0 + (\beta_j - \beta_0)\frac{\delta z}{\Delta z}$, being (α_0, β_0) the twist and bending angles of the current configuration and $\mathbf{c}_{(i,j)} = (\alpha_i, \beta_j)$ those that produce the lowest cost value K when a step Δz is advanced.

During the virtual exploration the user is who takes the control of the motions, i.e. step 3.4. is performed by the user manipulating the haptic device. To help him/her in this task, the best motion computed by the algorithm in step 3.3. is continually suggested to the user, both visually and haptically.

The average time to compute the best motion (steps 3.1. to 3.3.) is 0.3 s, fast enough for the user to feel he is

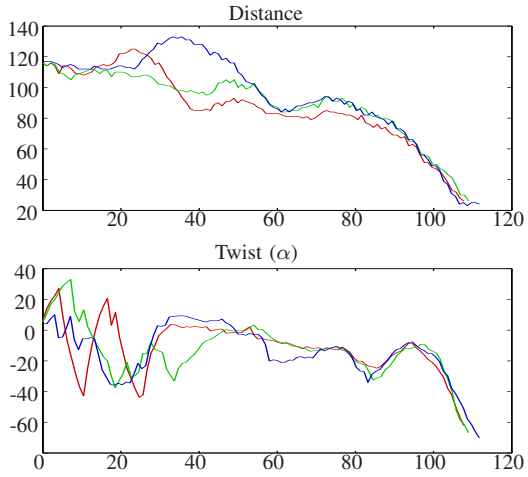

Fig. 6. Distance and twist values along a solution path for different weights values $(\omega_{NF1}, \omega_{cl}, \omega_\alpha)$: red (1,0,0), green (0.6,0.2,0.2), blue (0.4,0.4,0.2).

Algorithm 2 Compute-path

Require:
Δz, δz: Advance steps
c_{ini}: Initial bronchoscope configuration
v_{goal}: Goal voxel
Ensure:
P: Solution path
reached: Result of the search

1. Compute clearance-based NF1 navigation function
2. $P \leftarrow c_{ini}$
while (bronchoscope TCP not in v_{goal}) **do**
  3.1. S = Compute (α, β) candidates using Δz (Eq (3))
  3.2. S_{valid} = Evaluate S
  if $S_{valid} = \emptyset$ **then**
    return $\{P$, reached=FALSE$\}$
  end if
  3.3. $\mathbf{c}_{(i,j)}$ = Choose candidate with lowest cost K (Eq (9))
  3.4. $c \leftarrow$ `MoveBronchoscope`
  3.5. $P \leftarrow c$
end while
return $\{P$, reached=TRUE$\}$

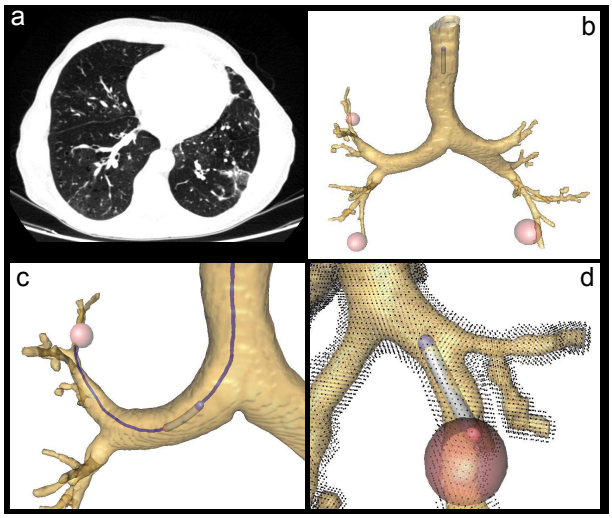

Fig. 7. a) CT image; b) triangular mesh reconstruction of the tracheo-bronchial tree with three lesions marked; c) Solution path to one of the selected peripheral lesions; d) Final configuration of the path.

receiving suggestions in real time during the interactive guided navigation.

VI. An example

The CT slices used are 0.6 mm thick, being the size of the smallest bronchia segmented of the 4^{rd} order, with an approximate diameter of 2.30 mm. Fig. 7a shows a CT-slice and Fig. 7b the VRML model of the reconstructed tracheobronchial tree. The resolution of the 3D image (i.e. the voxels size) is $0.7 \times 0.7 \times 0.6$ mm and there are 116,758 interior voxels, being the voxel with more clearance located at a L1 distance of 13. The time to compute the clearance-based NF1 navigation function has been 10 s.

Three peripheral lesions have been selected as tests. Fig. 7c shows a path towards one of them, and Fig. 7d a detail of the final configuration where the grid is visible (see the accompanying video for an animation of the path). The algorithm was called with $\Delta z = 5$ mm and $\delta z = 1$ mm. The time to compute the solution path to this lesion has been 31 ± 2 s (10 executions have been performed to take into account the randomization in the definition of the look-at points).

Fig. 8 shows the haptic-based haptic exploration of the tracheobronchial tree towards that lesion, using the output of the planning module.

VII. Conclusions

This paper has presented a planning module within the scope of a haptic-based virtual bronchoscopy system with a guiding aid. The planner takes into account the geometry and the kinematic constraints of the bronchoscope and computes a path from an initial configuration located at the trachea towards a selected peripheral lesion. This path can be simulated providing a realistic fly-through execution of the bronchoscopy prior to the virtual exploration using the haptic device. During the exploration the planning module is able to provide the best motion to be followed towards the goal from any configuration the user might be, as well as the approximate cost of the motion selected by the user, that is transformed into a force feedback, thus facilitating some motion directions and hampering others.

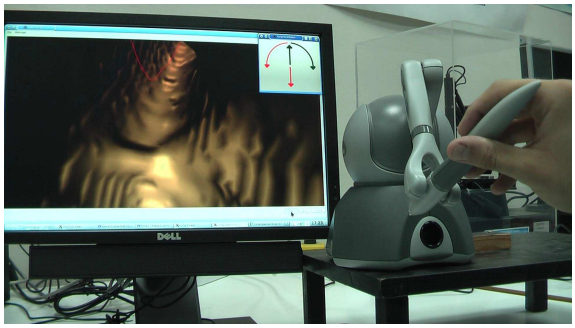

Fig. 8. Haptic-based guided exploration.

References

[1] N. Shinagawa, K. Yamazaki, Y. Onodera, K. Miyasaka, E. Kikuchi, H. Dosaka-Akita, and M. Nishimura, "CT-guided transbronchial biopsy using an ultrathin bronchoscope with virtual bronchoscopic navigation," *CHEST*, vol. 125, no. 3, pp. 1138–1143, 2004.

[2] J. Ferguson and G. McLennan, "Virtual bronchoscopy," *Proceedings of American Thoracic Society*, vol. 2, pp. 488–491, 2005.

[3] P. Cabras, J. Rosell, A. Pérez, W. G. Aguilar, and A. Rosell, "Haptic-based navigation for the virtual bronchoscopy," in *Proc. of the IFAC World Congress*, 2011.

[4] A. P. Kiraly, J. Helferty, E. Hoffman, G. McLennan, and W. Higgins, "Three-dimensional path planning for virtual bronchoscopy," *IEEE Trans Med Imaging*, vol. 23, pp. 1365–1379, 2004.

[5] M. Negahdar, A. Ahmadian, N. Navab, and K. Firouznia, "Path planning for virtual bronchoscopy," in *Proc. of the 28th IEEE EMBS Annual Int. Conf.*, 2006, pp. 156–159.

[6] M. Moll and L. Kavraki, "Path planning for deformable linear objects," *IEEE Trans. Robotics*, vol. 22, no. 4, p. 625636, 2006.

[7] R. Gayle, P. Segars, M. Lin, and D. Manocha, "Path planning for deformable robots in complex environments," in *In Robotics: Systems and Science*, 2005.

[8] S. P. E. Lobaton, J. Zhang and R. Alterovitz, "Planning curvature-constrained paths to multiple goals using circle sampling," in *Proc. of the IEEE Int. Conf. on Robotics and Aut.*, 2011, pp. 1463 – 1469.

[9] S. Patil and R. Alterovitz, "Interactive motion planning for steerable needles in 3d environments with obstacles," in *Proc. of the IEEE RAS/EMBS Int. Conf. on Biomedical Robotics and Biomechatronics*, 2010, pp. 893–899.

[10] A. Shkolnik, M. Walter, and R. Tedrake, "Reachability-guided sampling for planning under differential constraints," in *Proc. of the IEEE Int. Conf. on Robotics and Automation*, 2009, pp. 4387–4393.

[11] A. Yershova and S. M. Lavalle, "Motion planning for highly constrained spaces," *Connect*, vol. 396, pp. 297–306, 2009.

[12] D. Berenson, T. Simeon, and S. Srinivasa, "Addressing cost-space chasms in manipulation planning," in *Proc. of the IEEE Int. Conf. on Robotics and Automation*, 2011, pp. 4561 – 4568.

[13] S. Sekhavat and M. Chyba, "Nonholonomic deformation of a potential field for motion planning," in *in Proceedings of IEEE International Conference on Robotics and Automation*, 1999, pp. 817–822.

[14] A. Masoud, "A harmonic potential field approach for navigating a rigid, nonholonomic robot in a cluttered environment," in *Proc. of the IEEE Int. Conf. on Robotics and Automation*, 2009, pp. 3993 – 3999.

[15] A. P. Kiraly, W. E. Higgins, G. Mclennan, E. A. Hoffman, and Reinhardt, "Three-dimensional human airway segmentation methods for clinical virtual bronchoscopy," *Academic Radiology*, vol. 9, no. 10, pp. 1153–1168, 2002.

[16] A. P. D. Babin, E. Vansteenkiste and W. Philips, "Segmentation of airways in lungs using projections in 3-D CT angiography images," in *Proc. of the 32nd Annual Int. Conf. of the IEEE EMBS*, 2010, pp. 3162–3165.

[17] AMIRA, http://www.amira.com/, 2010.

[18] J. C. Latombe, *Robot Motion Planning*. Kluwer Ac. Publishers, 1991.